A Study of b-value Precursors Applied to the Andaman-Sumatra Region

Article · January 2012

CITATIONS
4

READS
360

2 authors:

Paiboon Nuannin
Prince of Songkla University
12 PUBLICATIONS **216** CITATIONS
SEE PROFILE

Ota Kulhánek
Uppsala University
62 PUBLICATIONS **910** CITATIONS
SEE PROFILE

Journal of Earth Science and Engineering 2 (2012) 166-188

A Study of *b*-value Precursors Applied to the Andaman-Sumatra Region

Paiboon Nuannin[1] and Ota Kulhánek[2]

1. Department of Physics, Faculty of Science, Prince of Songkla University, Hatyai 90112, Thailand

2. Department of Earth Science, Uppsala University, Uppsala SE-752 36, Sweden

Received: January 4, 2012 / Accepted: February 10, 2012 / Published: March 20, 2012.

Abstract: The temporal and spatial FMD (frequency-magnitude distribution) of earthquakes in the Andaman-Sumatra region is analyzed. Four earthquake catalogs have been used namely the ISC, NEIC, IDC and HRVD catalogs comprising between 1,107 and 13,672 events. Temporal variations of *b*-values, *b(t)*, are investigated using sliding time windows containing 50 events with 5 event shifts at a time. The results reveal that large earthquakes occur when *b* decreases by more than ~0.3-1.0, suggesting that variation of *b* can be used as a medium-term (months-years) earthquake precursor. Spatial variations of *b*-values in the region are mapped by estimating the *b*-value at every 0.5° × 0.5° grid node using the nearest 50 events. Mapping of *b* provides information about the state of stress of the region, i.e. major *b*-value anomalies (low *b*) indicate epicentral areas of large earthquakes. During the studied period, large earthquakes occurred in areas of low value of *b* (*b~ 0.5-1.1*). On the other hand, no large earthquakes were observed in high *b*-value (*b~1.2-2.2*) areas. Areas of major *b* anomalies are found at latitude 0°-15°N, i.e. north of the two giants shocks M_w = 9 and M_w = 8.7, at 4°S-2°S and at 5°S-7°S or around and southeast of the M_w = 8.7 epicenter areas. *b*-values in the epicentral areas increase after the two mainshocks, suggesting that changes of *b(t)* can also be used as a short-term (days-months) earthquake precursor for aftershock sequences.

Key words: *b*-value, earthquake precursors, Andaman-Sumatra, giant shock, aftershock series.

1. Introduction

Various seismic precursors have earlier been studied by many investigators for the purpose of earthquake prediction. For example, Ogata et al. [1], among others, studied the precursory quiescence time as a means of predicting earthquakes. Mogi [2] analyzed the space and time distribution of seismicity. Precursory changes in source parameters such as corner frequency, stress drop and fault radius were reported by Jain et al. [3] or by Urbancic and Young [4]. Evison and Rhoades [5-7] carried out studies of swarms and found precursory behavior related to major earthquakes. Molchan and Dmitrieva [8] investigated the temporal variation of *b* of foreshock series preceding the mainshock by some hours to days.

Corresponding author: Paiboon Nuannin, lecturer, Ph.D., main research fields: earthquake precursors, seismic hazard assessment, seismicity analysis. E-mail: paiboon.n@psu.ac.th.

The present study is focusing on determination of the *b*-value as a function of time and space for events in the Andaman-Sumatra region and on assessment of its potential as a seismic precursor. Earthquake data for time period 1/1/1995-26/12/2004 from four different earthquake catalogs are used.

The frequency of earthquake occurrence in a given area during a specific period of observation can be expressed as a function of magnitude through a relation given by Gutenberg and Richter [9]

$$\log N = a - bM \quad (1)$$

where N is number of earthquakes within the magnitude interval $M \pm \Delta M$ (interval distribution), a and b are positive real constants. For a cumulative distribution, applied in the present study, N refers to a number of events with magnitudes equal to or larger than M. The parameter a shows the activity level of seismicity and exhibits significant variations from

region to region. It also depends on the period of observation and the size of area of investigation. The parameter *b* is related to tectonic structure and depends upon the stress regime of the studied region [10-13]. Calculation of *b* for different regions is restricted to the magnitude range $M_{min} \leq M \leq M_{max}$, where M_{min} is a threshold magnitude of complete catalogs. Confidence limits of the *b*-value are inversely proportional to the square root of the number of events [14]. The frequency-magnitude distribution (Eq. (1)) deviates from linearity at low and at high magnitude. Deviation at low magnitudes is due to the limited sensitivity of the monitoring seismic networks. Deviation at high magnitudes occurs because of the saturation of magnitude scales leading to inadequate (low) numbers of large earthquakes, i.e. to an abrupt decrease in the magnitude-frequency distribution [15].

On average, *b* is nearly unity for most seismically active regions on Earth [16]. However, for shorter time windows and limited geographical areas, statistically significant variations have been observed. High *b*-values are observed in regions of (a) decreased shear stress; (b) high slip release on earthquake rupture planes; (c) extensional stress; (d) high pore pressure and (e) fault creep [17]. Low *b*-values are often associated with major earthquakes and highly stressed asperities [18]. Observations reveal a high spatial variability of *b*, even on a scale of few kilometers.

Changes in *b*-value preceding major shocks have been reported and supported by evidence from laboratory studies by Scholz [19]. The inverse correlation between the amount of stress accumulated in the hypocentral volume and the *b*-value is obviously of particular interest in the prediction of major earthquakes. Variations of *b*-values with durations of months and years are known to precede large shocks in various parts of the world. In Japan, Imoto [20] found that decreases in *b*-values appeared a few years before earthquakes with magnitude 6.0 and greater. He considers the decrease in *b*-values as a promising precursor candidate since during a period preceding the occurrence of major earthquakes, the decrease appears more frequently than might be expected from a random chance. Sahu and Saikia [21] observed a short-term drop in *b* before the occurrence of the August 6, 1988 earthquake (M_s = 7.3) in the India-Myanmar border region. More examples can be found in the literature.

The *b*-value of a set of events may be estimated by linear least-squares regression or by the maximum likelihood method. Aki [14] presents the maximum likelihood estimate of the *b*-value as

$$b = \frac{\log_{10} e}{\overline{M} - M_{\min}} \tag{2}$$

where $\overline{M}$ is the mean magnitude above the threshold M_{min}. An estimate of the standard deviation δb of the *b*-value can be obtained by using the formulation by Shi and Bolt [22]

$$\delta b = 2.3 b^2 \sqrt{\sum_{i=1}^{n} (M_i - \overline{M})^2 / n(n-1)} \tag{3}$$

where *n* is the number of events of the given sample.

The Andaman-Sumatra region, which is one of the most active seismic regions, has been studied earlier by several authors [23-25]. The inverse correlation between the amount of stress accumulated around the hypocentre and the *b*-value was investigated by Nuannin et al. [26] by employing earthquake data during a five year period preceding the giant shock on December 26, 2004. The results show that *b*-values drop significantly prior to the occurrence of two large events in 2002 and prior to the devastating shock of 2004.

In this study, the area of investigation is centered at the epicenter of the 2004 (M_w = 9.0) earthquake off the coast of NW Sumatra and extends about 15° degrees to the north and 15° to the south. *b*-value is determined as a function of time and space for events during the time period 1995-2005. Spatial and temporal *b* variations are examined retrospectively as possible precursors heralding an occurrence of major earthquakes in the Andaman-Sumatra region. Aftershock series of the 2004 (M_w = 9.0) and the 2005 (M_w = 8.7) events are also examined. Results based on different earthquake

catalogs are compared.

2. Investigated Area

The Indo-Burmese range and the Andaman arc system in the northeast Indian Ocean are defined as a zone of underthrusting of the Indian plate below the Southeast Asian plate, leading to the formation of a major island arc-trench system (Fig. 1). The Andaman Sea extends from Myanmar in the north to Sumatra in the south and from the Malay Peninsula in the east to the Andaman and Nicobar islands in the west [27].

Subduction of the Indian plate along the Andaman arc, formation of the Andaman Nicobar ridge and initiation of the spreading in the Andaman Sea are

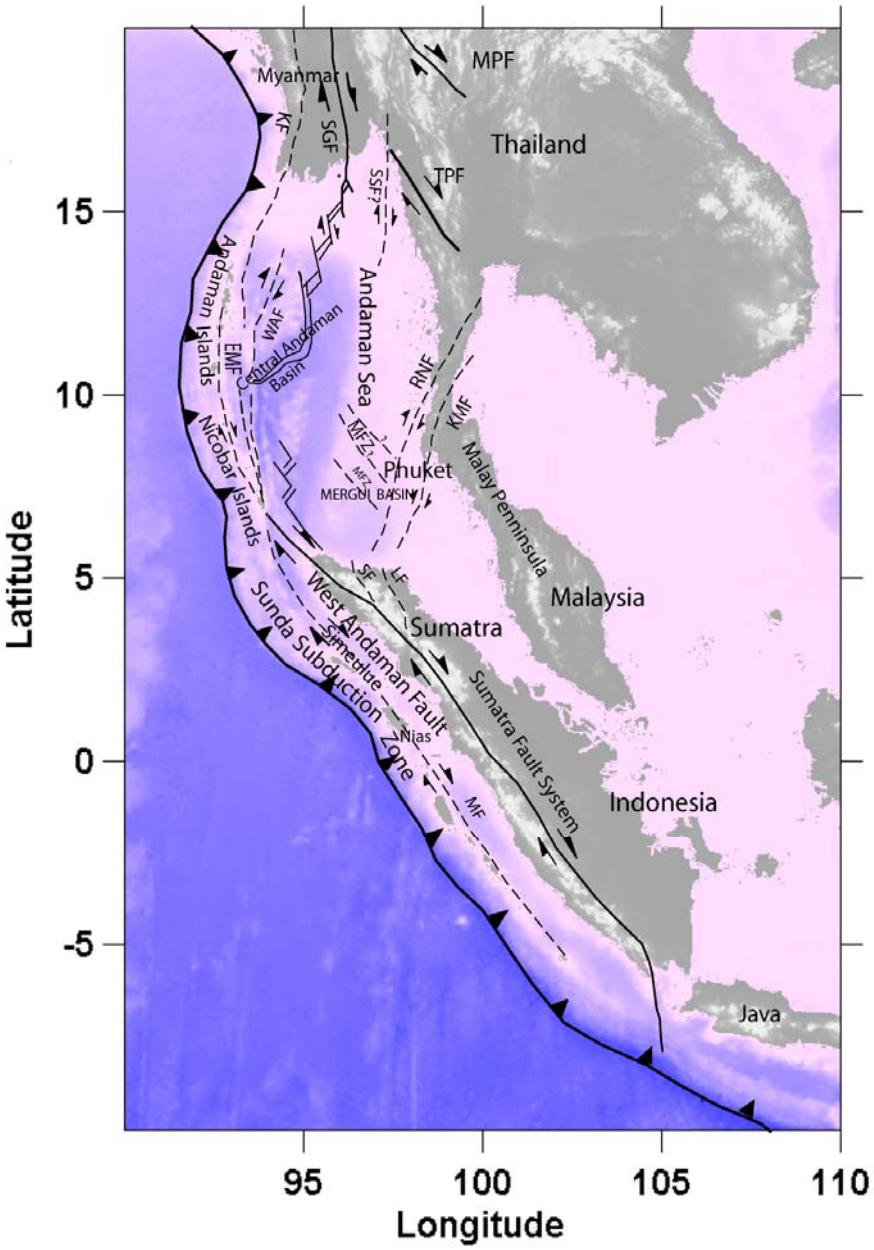

Fig. 1 Tectonics of the Andaman-Sumatra Region: EMF = East Margin Fault, KF = Kabaw Fault, KMF = Klong Marui Fault, LF = Lhokseumawe-Lopok Kutacane Fault, MF = Mentawei Fault, MFZ = Mergui Fault, MPF = Mae Ping Fault, RNF = Ranong Fault, SF = Samalanga Sipokok Fault, SGF = Sagaing Fault, SSF = Shan Scarp Fault, TPF = Three Pagodas Fault, WAF = West Andaman Fault [33, 34].

some of the important tectonic characteristics that shaped the Andaman backarc basin. Subduction is presumed to have started along the western Sunda arc following the break-up of the Gonwanaland in the early Creaceous [28]. Spreading rifts and transforms in the central basin of the Andaman Sea are connected to the Sagaing fault system in the Burma highlands in the north and to Semengko fault system in the south that longitudinally bisects Sumatra [29].

The Andaman Sea is a pull-apart basin located between two dextral strike-slip faults: the N-S trending Sagaing Fault in the north and the NW trending Great Sumatra Fault, which connects with the Andaman fault in the south. The faults formed in response to the relative oblique convergence between the Indian Plate and Sundaland. For most of the trench, they accommodate the parallel component of the motion between the two plates. The deformation is not restricted to a single fault but rather affects the entire Burma microplate with distributed dextral faults parallel to the Sagaing fault system and distributed NS trending folds accommodating the EW compressional component [30].

Sumatra is situated on the southern edge of the Sundaland north of Sunda Trench. The Sumatran Arc has a classic morphology of trench, accretionary prism, outer-arc ridge, forearc and volcanic chain with active andesitic volcanism [31] and there is a well defined Wadati-Benioff zone. The subduction direction changes from oblique to almost orthogonal between north Sumatra and Java, and India Sundaland motion is partitioned into trench-normal subduction and dextral slip on the Sumatran Fault and related strand [32]. Seismicity in the study region is high and associated with Sunda subduction zone, Andaman transform faults, Sumatra backarc and Sumatra fault system (Fig. 1).

3. Data and Analysis

Earthquake data employed in this study are retrieved from different sources that can be freely downloaded from their respective web sites. They include earthquake catalogs from the ISC (International Seismological Centre), IDC (International Data Centre), NEIC (USGS National Earthquake Information Center) and HRVD (Harvard CMT). These catalogs are different in magnitude scale, period of availability and number of reported events as shown in Table 1. The analysis started with earthquakes of magnitude $M \geq 4.1$ (except for IDC where $M \geq 3$ were used) in the area delimited by 10°S-20°N and 90°-110°E that covers the whole Andaman-Sumatra region. Small events (M usually less than 4) are often reported with local magnitudes from different agencies usually without any specification and cannot enter the present analysis. Moment magnitudes, M_w, for ISC and NEIC lists were derived from reported m_b using linear relationships based on parallel m_b and M_w reported in IDC lists because no M_w are reported in the IDC catalog. Hence, for IDC, m_b is used. Most of listed magnitudes in the study area in the IDC are below 6.5.

Only two events have larger magnitude, i.e. 6.6 and 7.2. Since saturation starts at m_b~6.5 [35] thus, the saturation effect is not a serious problem here. Earthquakes of all depths ranging from 0-650 km are used in the analysis. The starting data sets used in the analysis are summarized in Table 1. As an example, Fig. 2 exhibits epicenters of earthquakes within the

Table 1 Parameters of catalogs used.

Catalog	Magnitude type	Time period	No. of events	*M
ISC	M_w	1/1/1964-31/12/2003	6,876	4.2
IDC	m_b	1/1/1995-17/08/2005	13,672	3.0
NEIC	M_w	1/1/1973-31/12/2005	10,840	4.1
HRVD	M_w	1/1/1977-19/11/2005	1,107	4.6

*M are chosen starting (lowest) magnitudes in respective catalog.

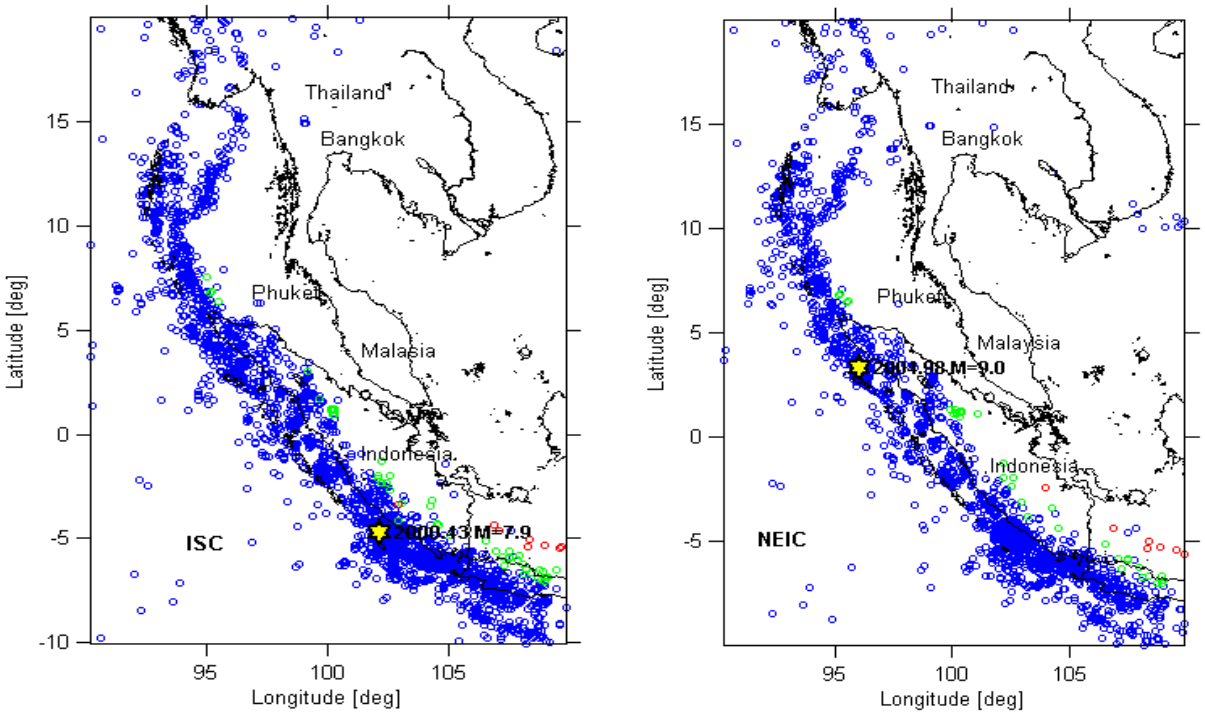

Fig. 2 Seismicity map of the studied area: (left) ISC (1964-2003, M_w > 5, n = 2,165 events), star shows the epicenters of maximum magnitude event in the catalog; (right) NEIC (1973-2005, M_w > 4.9, n = 2,125 events), star shows the epicenter of the M_w = 9.0 event of December 26, 2004, i.e. the largest event in the catalog.

studied area reported in the ISC and NEIC catalogs. As follows from the figure, the distribution is similar for both catalogs in spite of different reporting time periods.

4. Declustering the Earthquake Catalogs

In order to analyze the expected anomalies in the spatial and temporal distribution of the seismic activity, the catalogs were declustered to remove "dependent" events. Since there is no standard procedure for aftershock removal, Reasenberg's [36] decluster method for aftershock identification was applied. Aftershock populations are identified by modeling an interaction zone around each earthquake in the catalog. Any earthquake that occurs within the interaction zone of a prior mainshock is classified as an aftershock and considered as a dependent event. Several parameters have to be chosen for the declustering procedure. A detailed description is given in Ref. [36] and in the ZMAP program manual [37].

Fig. 3 shows cumulative number of original and declustered data sets for ISC and NEIC catalogs. Examination of the cumulative number of events in the catalogs reveals a change in the rate of detected events between 1985-1999 and 2000-2004. This is most likely due to the improving delectability of seismic networks and methods of computing. To avoid the numerous aftershocks of the M_w = 9 December 26, 2004, shock, data from each catalog is limited by 26/12/2004, hereafter to be referred to as 2004.98. Numbers of earthquakes in the original catalogs are respectively 6,876 and 6,171 for the ISC and NEIC catalogs. Earthquakes remaining in the declustured catalog are 6,071 and 4,752, respectively. The aftershock data are investigated separately for spatial and temporal variation of *b*.

5. Completeness of Catalogs

An assessment of the minimum magnitude of complete recording, the so-called threshold magnitude, M_c, is an important part of data quality control. M_c is defined as the lowest magnitude for which all events in

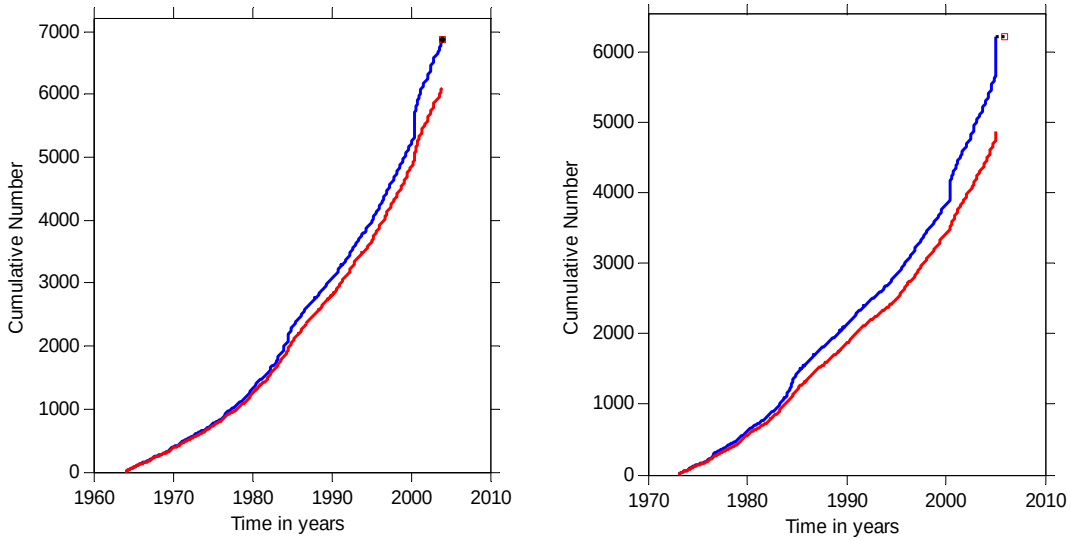

Fig. 3 Cumulative number of events of original (blue) and declustered catalogs (red): (left) ISC: 1964-2003; (right) NEIC.

a studied space-time volume are detected. M_c varies with space and time. For most catalogs it decreases with time, because the number of monitoring seismographs continuously increases and the analysis methods improve [38, 39]. The magnitude of completeness of the declustered catalogs was determined by the Best Combination method in the ZMAP software. Time series of M_c are computed by means of overlapping moving windows to reveal the possible time dependence of M_c. Windows contain 300 events stepped by 100 events, except for the HRVD catalog where analysis contained 100 events and stepped by 20 events in order to maximize the number of results.

Fig. 4 displays M_c as a function of time for the four catalogs. As can be seen in the figure, the threshold magnitude is highest (worst) for the HRVD catalog (M_c ~ 5.2) and lowest (best) for the IDC catalog (M_c ~ 3.9). Results from the ISC and NEIC catalogs are comparable with M_c changing from 5.2 in an early period to 5.0 in the mid 1980s and gradually decreasing to about 4.7 in 2000. Consequently, the deduced M_c for the ISC and NEIC catalogs are 5.0 and 4.9, respectively, whereas IDC and HRVD, respectively were assigned M_c = 3.9 and M_c = 5.2.

6. Temporal Changes of *b*-values?

Temporal changes of *b*-values have earlier been

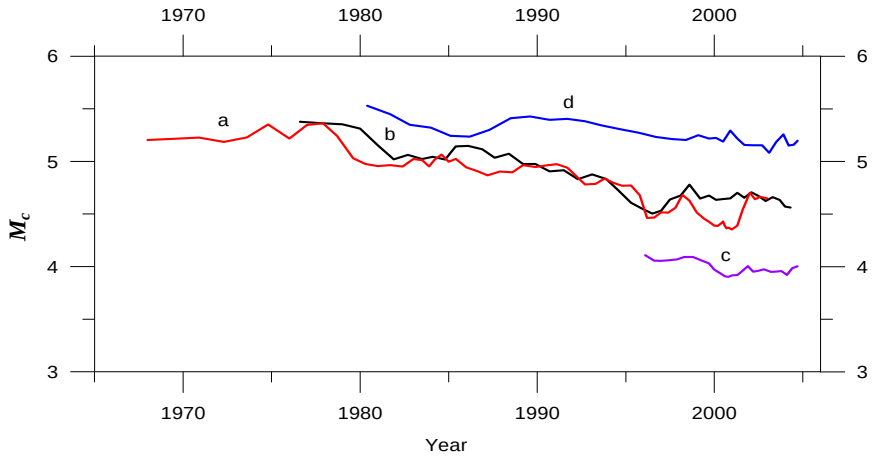

Fig. 4 M_c as a function of time for the four catalogs used: a = ISC; b = NEIC; c = IDC and d = HRVD.

investigated by other authors and some studies have focused on both the spatial and temporal variability of *b* simultaneously. Short-term (weeks) temporal variations in *b* for mining tremors have been used for hazard analysis [40-42]. Wiemer and Wyss [43] observed a temporal *b*-value change with high statistical significance between creeping segment and asperity of the Parkfield segment of the San Andreas fault. They also noticed an increase in *b* correlating with magmatic intrusions beneath the Off-Izu volcano and beneath Mammoth Mountain. These three cases were all step-function-like increases and were associated with a major redistribution of stress or injection of fluid into a seismogenic volume. Long period changes (months-years) of *b* also do occur. Jones and Hauksson [44] showed that the *b*-value in southern California was lower before the 1952 Kern County earthquake compared to levels after the events. The hypothesis that seismic moment release rate (accelerating rate) increases regionally before large earthquakes implies that *b* should be anomalously low before the occurrence of the events [45].

To examine a possible long-term temporal change of *b*, the ISC, IDC and NEIC catalogs were subdivided into two periods, each covering 5 years, i.e. 1995-1999 and 2000-December 26, 2004. The HRVD catalog is not divided because it includes a small number of events. *b(t)* is calculated in sliding time windows containing a constant number, *n*, of events. The window is moved in time by an *n/10* increment of event counts. The choice of the number of events in each window is a compromise between the time resolution and the smoothing effect of broad windows [21, 26, 46]. The windows were employed with 50 events and 5 event increments. Calculations and a plot of *b* as a function of time, *b(t)*, were performed using the ZMAP software package [47].

Average overall *b*-values of the employed data sets are summarized in Table 2. The highest value, $b = 1.38$, of ISC is likely to be due to lack of data for the year 2004. The present investigation is focused on the relative variation of *b*, and so the absolute values are of less importance.

7. Spatial Variations of *b*-values

The magnitude-frequency distribution as a function of spatial position can be mapped by projecting earthquake epicenters onto a plane. The *b*-value is estimated at every node of a plane grid, using the *N* (*N* = constant) nearest earthquakes, or a varying number of events located within a chosen (constant) distance, *R*, from the node. When *N* is constant, it is usually in the range of 50-500 events, and the nodal separation is 0.1°-1°, depending on the density of epicenters. To visualize the variation, *b*-values are translated into a color code and plotted for each grid node.

In a previous study [26], a five-year period preceding the giant shock of December 26, 2004, containing 624 earthquakes in the Andaman-Nicobar Islands region was used for a *b*-value anomaly investigation. The results demonstrate that *b*-value decreased significantly in and around the epicentral areas of the $M_w = 9$, December 26, 2004 and the $M_w = 8.7$, March 28, 2005 events. In the present study, earthquake data from four catalogs (Table 1) are used for evaluation of *b*-values in the Andaman-Sumatra region. Earthquakes covering the whole period of each catalog (Table 2) are employed for *b*-value mapping (Fig. 5). As follows from the table, the available period of data is different for each catalog. To make

Table 2 Average *b*-values of data sets used and magnitudes of completeness.

Catalog	Time period	Magnitude scale	No. of events	*b*-value	M_c
ISC	1964-2003	M_w	6,071	1.38 ± 0.03	5.0
IDC	1995-2004.98	m_b	5,635	1.21 ± 0.03	3.9
NEIC	1973-2004.98	M_w	4,752	1.19 ± 0.03	4.9
HRVD	1977-2004.98	M_w	675	0.97 ± 0.04	5.2

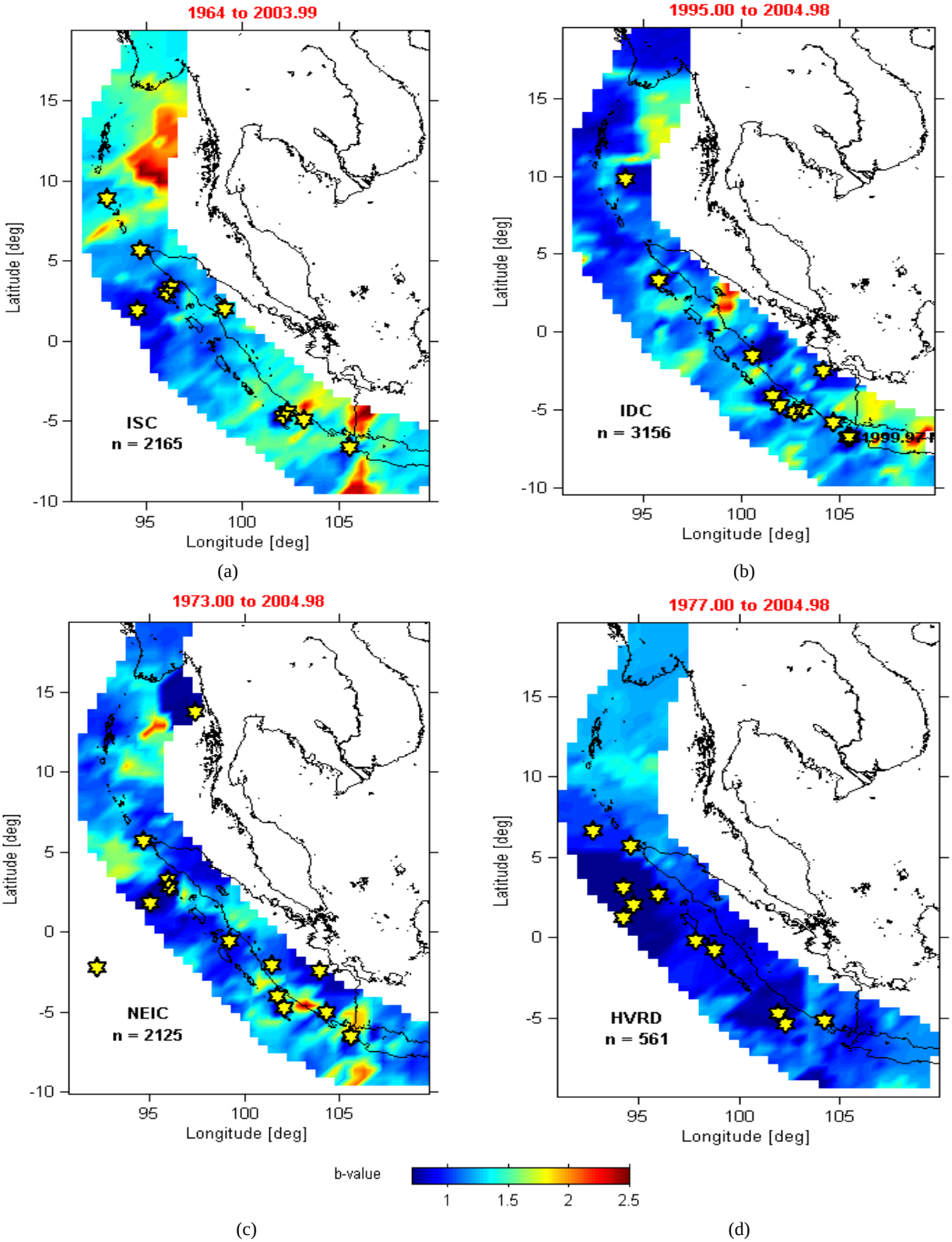

Fig. 5 ***b*-values in the studied region determined from different earthquake catalogs: (a) ISC, (b) IDC, (c) NEIC and (d) HRVD. Time periods covered are given on top of each map, n = number of earthquakes, $M \geq M_c$, used. Stars indicate the largest events in each catalog (see Table 3) during the respective time period. Note that the large events (stars) occur in areas of low *b* (blue color).**

comparison possible, the time window applied has been limited to 1995-2004.98 and subsequently subdivided into two five-year periods, i.e. 1995-1999 and 2000-2004.98 to reveal a possible time dependent re-distribution of *b*.

The study area is subdivided into a 0.5° × 0.5° grid to examine the spatial distribution of *b*. *b*-values are calculated for circular areas centered at grid nodes. Radii of circles vary along the grid in order to contain the prescribed constant number of 50 earthquakes. Also mapped are the radii of each circle employed to measure the achieved resolution. The *b*-values are calculated by a least-square linear fit and a magnitude increment $\Delta M = 0.1$ is applied throughout the present work. The general trend of the results is checked by calculating *b* also by the maximum likelihood method. M_c is estimated separately for each sample, because it may vary as a function of location.

8. Results and Discussion

8.1 General b-value Map

An overall *b*-value map deduced from earthquakes ($M \geq M_c$) of the four declustered catalogs (see Tables 1 and 2) reveals a significant spatial variability of *b* (Fig. 5). Stars in the figure show epicenters of the largest earthquakes (Table 3), which occurred in the studied region during the time period given on top of each map. As follows from Fig. 5 all of these shocks appeared in areas of low *b*-values (blue color). On the other hand, there are no large earthquakes in high *b*-value areas (yellow/red color).

8.2 Resolution Map

Geographical resolution of *b* depends on a density of earthquakes associated with each grid node. Since the number, *N*, of nearest earthquakes is fixed at 50 events, the resolution varies inversely with the radius containing *N* events. Fig. 6 displays the resolution for the ISC, IDC, NEIC, and HVRD catalogs. For the first three catalogs, resolutions are about 50-100 km in the central area along the Sunda forearc. For the HRVD catalog, it is about 100-200 km due to the low number (561 events) of earthquakes in the declustered catalog. Low resolution appears in all catalogs north of 15°N,

Table 3 List of the largest earthquakes and their epicenters (Lat, Lon) from the four catalogs used.

Event No.	Catalog			
	ISC	IDC	NEIC	HRVD
1	1964.71 M_w = 6.6 93.03, 8.90	1995.85 m_b = 5.9 103.17, -4.98	1983.26 M_w = 6.8 94.82, 5.77	1979.74 M_w = 6.9 94.24, 1.23
2	1969.89 M_w = 6.7 94.61, 1.94	1999.62 m_b = 5.9 105.46, -6.75	1994.13 M_w = 6.9 104.30, -4.90	1983.26 M_w = 7.0 94.65, 5.72
3	1971.27 M_w = 6.6 102.32, -4.41	1999.97 m_b = 6.2 104.67, -5.84	1995.76 M_w = 6.8 101.43, -2.04	1984.88 M_w = 7.1 97.84, -0.23
4	1976.47 M_w = 6.6 96.28, 3.40	2000.43 m_b = 6.2 101.95, -4.68	1995.85 M_w = 6.9 101.43, -2.04	1994.13 M_w = 6.9 104.27, -5.15
5	1983.26 M_w = 6.8 94.72, 5.70	2000.82 m_b = 6.0 105.56, -6.75	1998.25 M_w = 7.0 99.26, -0.54	1995.85 M_w = 6.9 94.77, 2.00
6	1987.31 M_w = 6.6 99.08, 2.02	2001.04 m_b = 6.1 101.59, -6.75	2000.43 M_w = 7.9 102.08, -4.72	1998.25 M_w = 7.0 98.84, -0.78
7	1995.85 M_w = 6.7 103.23, -4.92	2004.14 m_b = 5.8 100.55, -1.50	2000.46 M_w = 7.9 97.45, 13.83	2000.43 M_w = 7.9 101.94, -4.73
8	2000.43 M_w = 7.9 102.14, -4.69	2004.43 m_b = 6.2 104.17, -2.47	2000.82 M_w = 6.8 105.63, -6.55	2001.12 M_w =7.4 102.36, -5.4
9	2000.82 M_w = 6.8 105.62, -6.65	2004.56 m_b = 5.8 104.17, -2.47	2001.04 M_w = 6.8 101.77, -4.02	2002.84 M_w = 7.3 95.99, 2.65
10	2002.84 M_w = 7.2 96.11, 2.97	2004.98 m_b = 6.6 94.11, 9.84	2002.84 M_w = 7.3 96.08, 2.82	2004.98 M_w = 7.2 92.79, 6.61
11	2003.72 M_w = 6.6 95.63, 19.87	2004.98 m_b = 7.2 95.78, 3.32	2004.56 M_w = 7.3 103.98, -2.42	2004.98 M_w = 9.0 94.26, 3.09
12			2004.98 M_w = 9.0 95.98, 3.29	

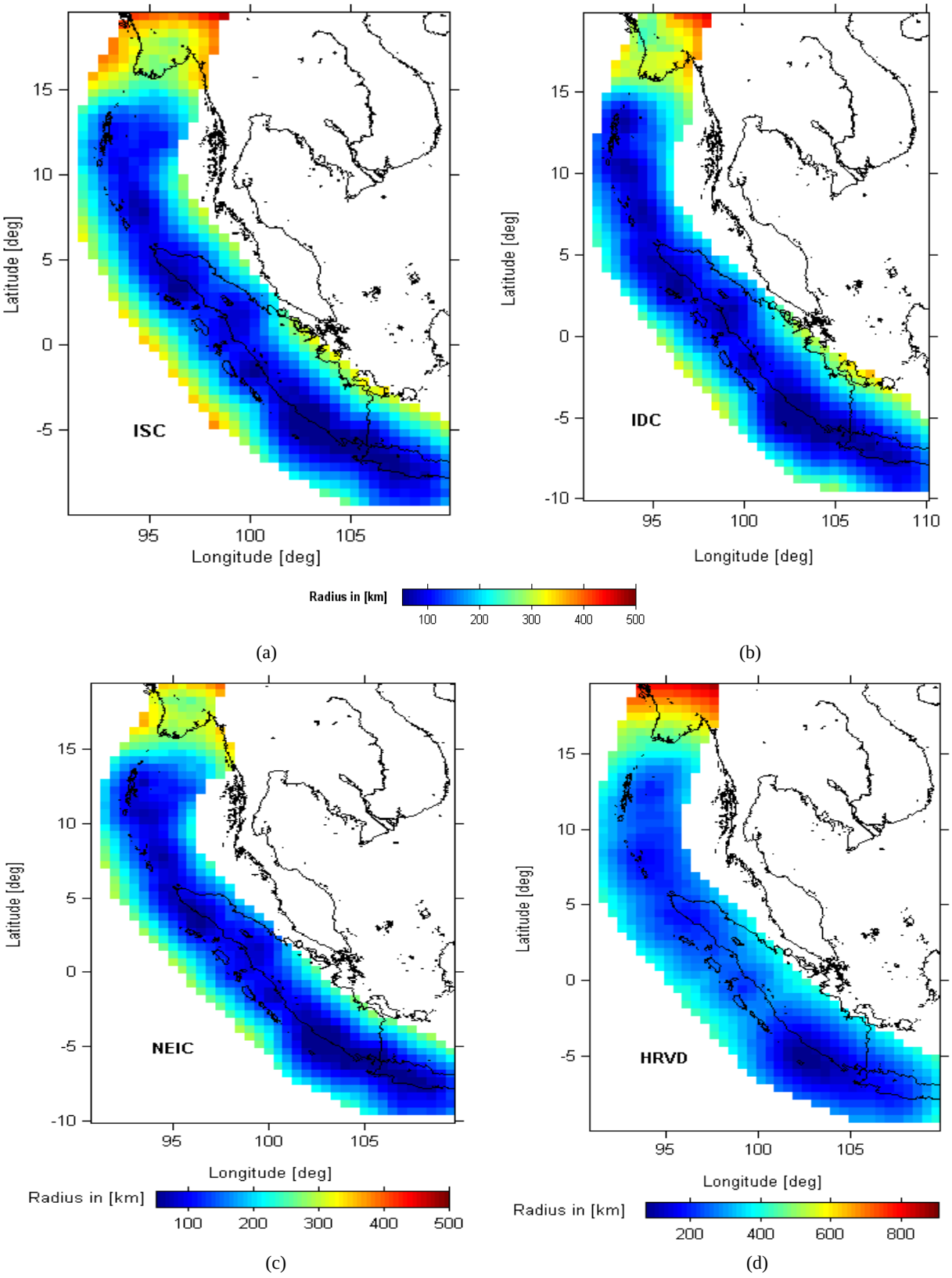

Fig. 6 Resolution maps for *b*-values exhibited in Fig. 5 for: (a) ISC, (b) IDC, (c) NEIC and (d) HRVD catalogs. Blue indicates high resolution, while red shows area with low resolution (for details see the text).

which is a low seismicity area.

8.3 Temporal and Spatial Distribution of b-values in Consecutive Five-Year Periods

The average *b*-value for the four catalogs is investigated for two five-year consecutive periods. Results and the number of earthquakes used, n ($M \geq M_c$), for estimation of *b*-values in time and space are presented in Table 4. As follows from the table, *b*-values for the first three catalogs decrease in the second five-year period, which is likely due to an occurrence of several large earthquakes in this period. Threshold magnitudes of each catalog are not different for the two five-year periods. Fig. 7 shows temporal variation of *b*-value, *b(t)*, separately for the first and for the second five-year period for the ISC, IDC and NEIC lists. For the HRVD catalog, *b(t)* is presented only for the whole period 1995-2004.98 due to a small number of earthquake data. Occurrences of large earthquakes are marked by arrows. As can be seen in the figure, large earthquakes occur when *b*-values decrease during the study period. This phenomenon is clear in the diagrams for each catalog. Significant drops (~0.8-1) appear in mid of year 1996, 1998, 2000, 2002, and in 2003 for the ISC catalog. For the IDC, the drops occur in 1996, 1997, 1998, 2000, and 2002 and at the end of 2004. Decrease of *b* for the NEIC catalog takes place in mid 1995, 1996, 2000, 2003 and at the end of 2004. For the HRVD *b* drops from about mid 2000 to the beginning of 2001 and at the end of 2004.

Fig. 8 displays the geographical distribution of *b*-values, during two five-year periods, left for 1995-1999 and right for 2000-2004.98. Stars mark epicenters of ten largest events that occurred during each period of the analysis. For the IDC catalog, the largest event magnitudes are $m_b > 5.4$ for both periods. For the other catalogs, the largest magnitudes are $M_w > 5.9$ and $M_w > 6.0$ for the period 1995-1999 and 2000-2004.98, respectively. Variation of *b*-values in the study region during the first and the second five-year period is recognized by the color code in the map. All large events occurred within the low *b*-value ($b < 1$, dark blue/blue color) areas, with *b*-value ranging 0.5-1. One should note that the average *b*-value of each catalog is different but the same color map scale is used in Fig. 8. In the NW Sumatra and Andaman-Nicobar islands area, latitude 0°-15°N, stress accumulated (*b*-values decreased) during the second period, i.e. during five years preceding the giant earthquakes, $M = 9$, of December 26, 2004 and $M = 8.7$, of March 28, 2005. Other two major changes of *b* in the first and the second five-year periods appear south of the two giant earthquakes, roughly the area of latitude 4°S-2°N and 5°S-7°S. In the former area (upper), *b* increases from ~1 to ~1.5, the *b* color map changes from dark blue to light blue. No large earthquake with magnitude greater than M_w *or* m_b specified in Fig. 8 took place during the time window considered. In the latter area *b* decreased from ~2.2 to ~1.2, the *b* color map changes to blue, i.e. the stress increase during the second period.

Table 4 *b*-values for consecutive five-year periods, *n* is a number of events, $M \geq M_c$.

Catalog	Time period	Magnitude type	*n*	*b*-value	M_c
ISC	1995-1999	M_w	857	1.23 ± 0.02	4.4
IDC	1995-1999	m_b	1,131	1.38 ± 0.02	4.1
NEIC	1995-1999	M_w	650	1.16 ± 0.03	4.5
HRVD	1995-1999	M_w	114	0.99 ± 0.02	5.1
ISC	2000-2003.99	M_w	942	1.11 ± 0.04	4.4
IDC	2000-2004.98	m_b	2,025	1.18 ± 0.02	4.1
NEIC	2000-2004.98	M_w	1,062	0.99 ± 0.08	4.5
HRVD	2000-2004.98	M_w	256	0.99 ± 0.07	5.1

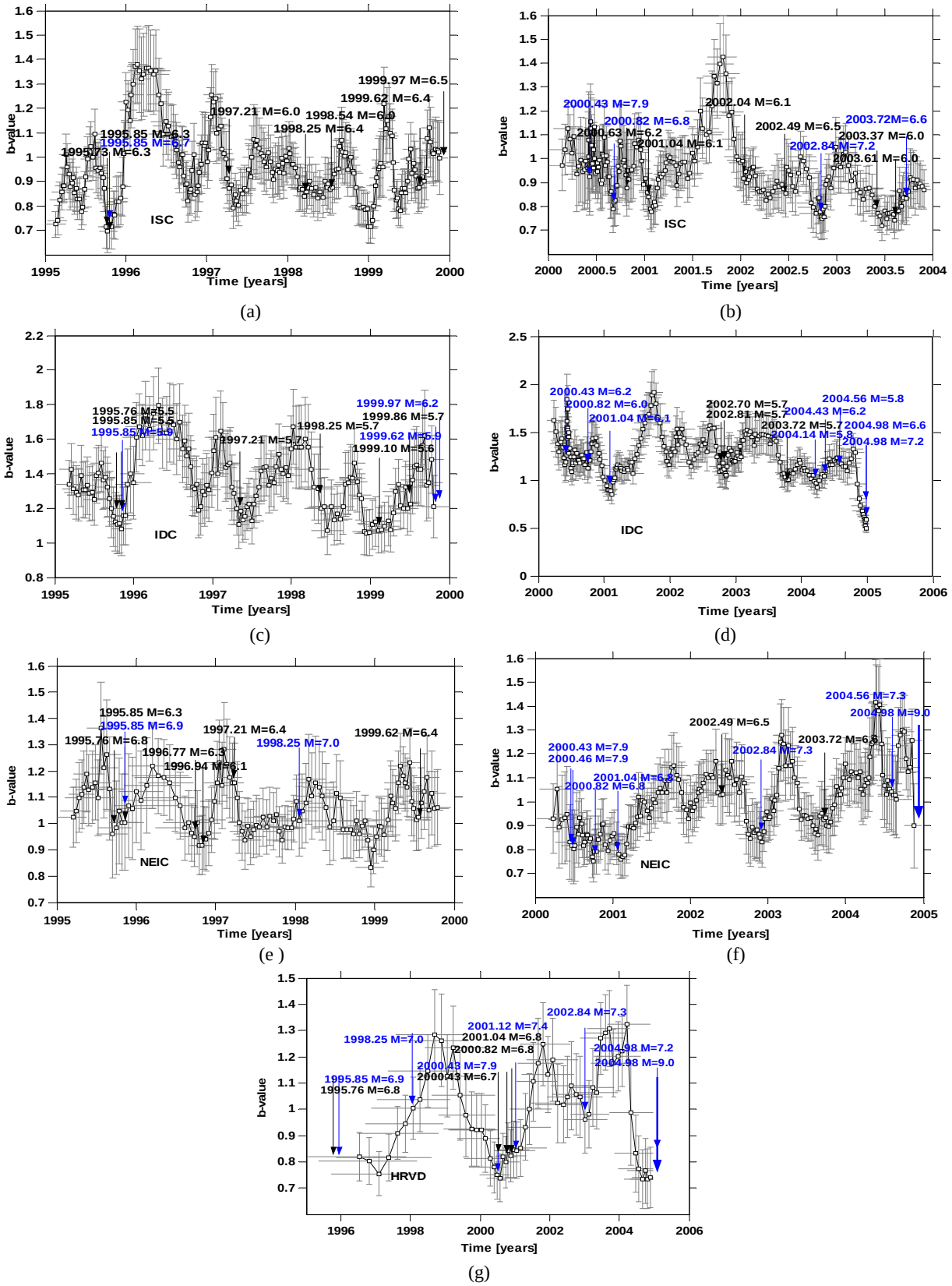

Fig. 7 ***b(t)*** **in the study region for time period 1995-1999 and 2000-2004.98, deduced from four different catalogs: (a-b) ISC, (c-d) IDC, (e-f) NEIC and (g) HRVD (1995-2004.98). Arrows show occurrence of large events. Blue arrows mark events listed in Table 3. Vertical bars indicate one standard deviation of the *b*-value, horizontal bars indicate sample period.**

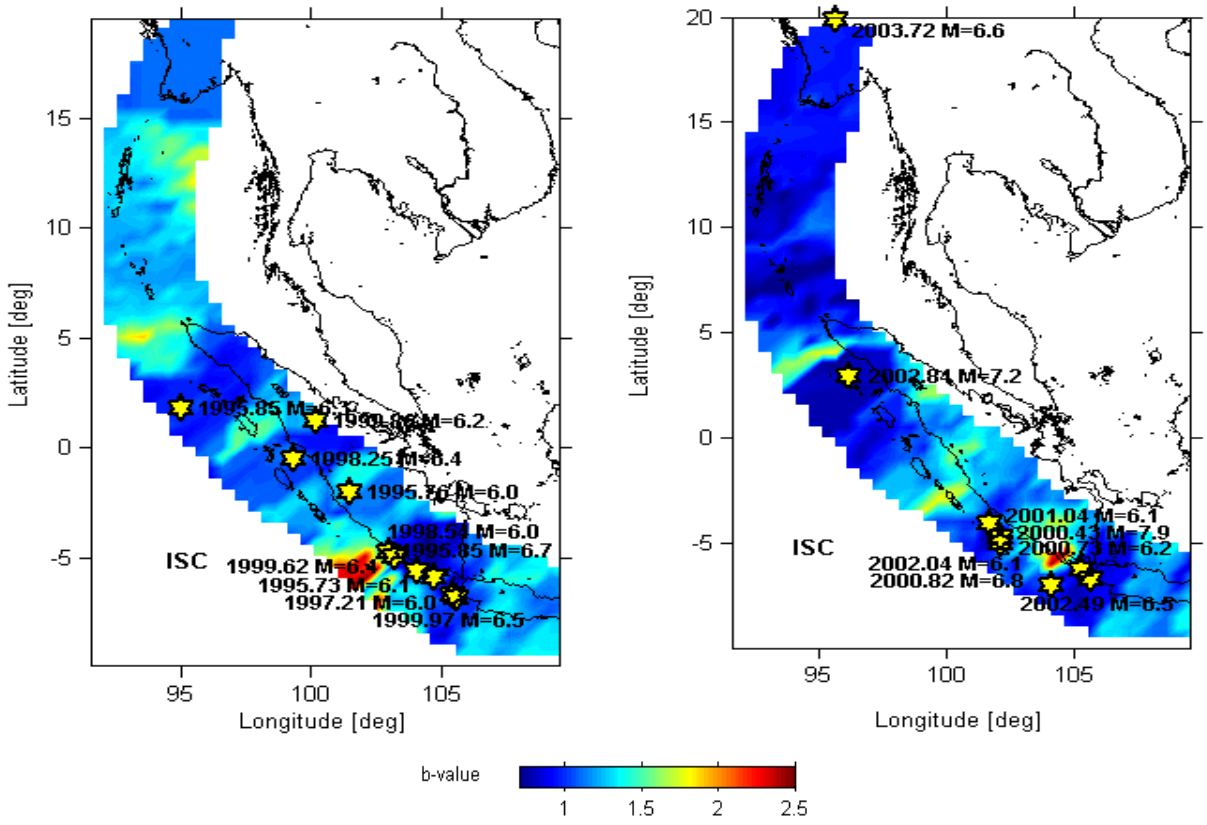
ISC
1995.85 M=6.2
1998.25 M=6.4
1995.76 M=6.0
1998.54 M=6.0
1995.85 M=6.7
1999.62 M=6.4
1995.73 M=6.1
1997.21 M=6.0
1999.97 M=6.5
2003.72 M=6.6
2002.84 M=7.2
2001.04 M=6.1
2000.43 M=7.9
2000.73 M=6.2
2002.04 M=6.1
2000.82 M=6.8
2002.49 M=6.5
Latitude [deg]
Longitude [deg]
b-value
1
1.5
2
2.5

(a)

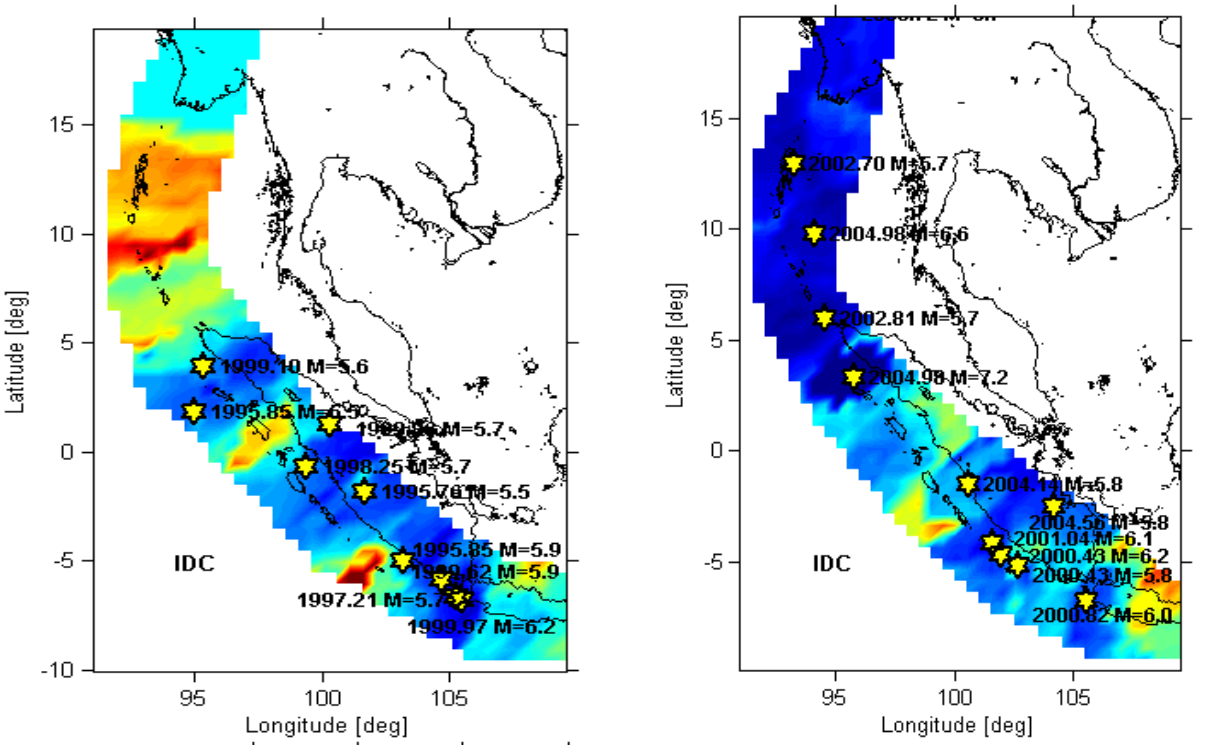
IDC
1999.10 M=5.6
1995.85 M=5.9
1998.25 M=5.7
1995.76 M=5.5
1995.85 M=5.9
1997.21 M=5.7
1999.97 M=6.2
2002.70 M=5.7
2004.98 M=6.6
2002.81 M=5.7
2004.98 M=7.2
2004.13 M=5.8
2001.04 M=6.1
2000.43 M=6.2
2000.43 M=5.8
2000.82 M=6.0
Latitude [deg]
Longitude [deg]

(b)

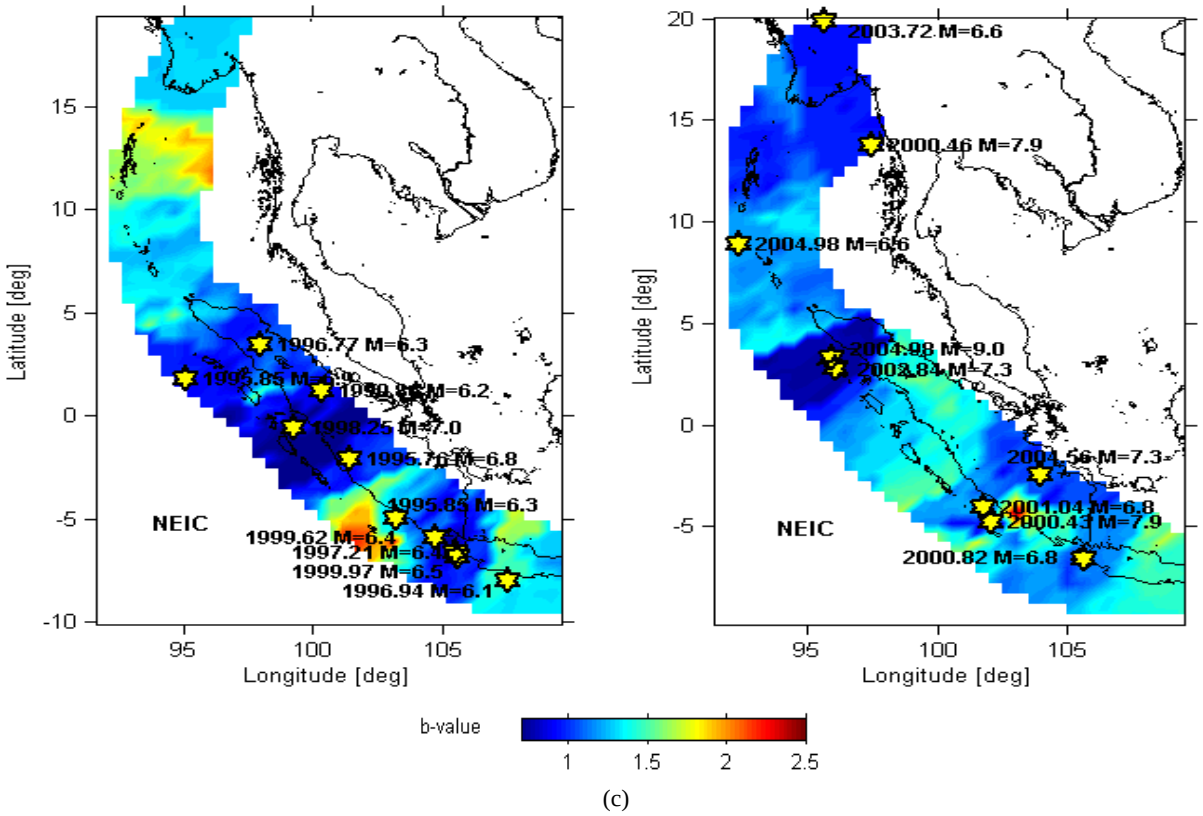

(c)

Fig. 8 Spatial distribution of *b*-values for two five-year periods, i.e. 1995-1999 (left) and 2000-2004.98 (right): (a) ISC, (b) IDC and (c) NEIC catalogs. Stars represent the 10 largest earthquakes in each period: left M_w > 5.9 for ISC, m_b > 5.4 for IDC and M_w > 6.0 for NEIC catalogs; right M_w > 6.0 for ISC, m_b > 5.6 for IDC and M_w > 6.5 for NEIC catalogs.

8.4 Temporal Variation of b for Selected Events

Two large events during the period 1995-2004.98 in each (ISC, IDC and NEIC) catalog were chosen for a detailed study of the variation of *b* with time in a limited area around the selected epicenters. To maximize the number of earthquakes entering the calculation and at the same time to avoid an interaction with other large near events, circular areas with 200 km radii centered at epicenters of the selected events were used. Details of the selected events used are given in Table 5. Fig. 9 shows epicentral maps of the earthquakes (green and red color) used. Plots of *b(t)* are displayed in Fig. 10. Results of *b*-values are summarized in Table 6, from which it follows that the events occurred when *b* dropped by about 0.4-0.6.

8.5 Aftershock Sequences

Earthquake sequences in the studied area following the Dec. 26, 2004 and March 28, 2005 shocks are here considered to be aftershocks. An epicentral map of the aftershocks is shown in Fig. 11. Time periods covered are listed in Table 7. The number of the events

Table 5 List of selected events.

Catalog	Event	Date	Location (Lat , Lon)	*M*
ISC	1	2000/06/04	-4.69, 102.14	$*M_w$ = 7.9
	2	2002/11/02	2.97, 96.11	$**M_w$ = 7.2
IDC	1	1999/11/11	1.30, 100.26	m_b = 5.7
	2	2002/11/02	2.92, 96.44	$**m_b$ = 5.5
NEIC	1	2000/06/04	-4.72, 102.08	$*M_w$ = 7.9
	2	2000/10/25	-6.55, 105.63	M_w = 6.8

**M* and ***M* are marked as the same events.

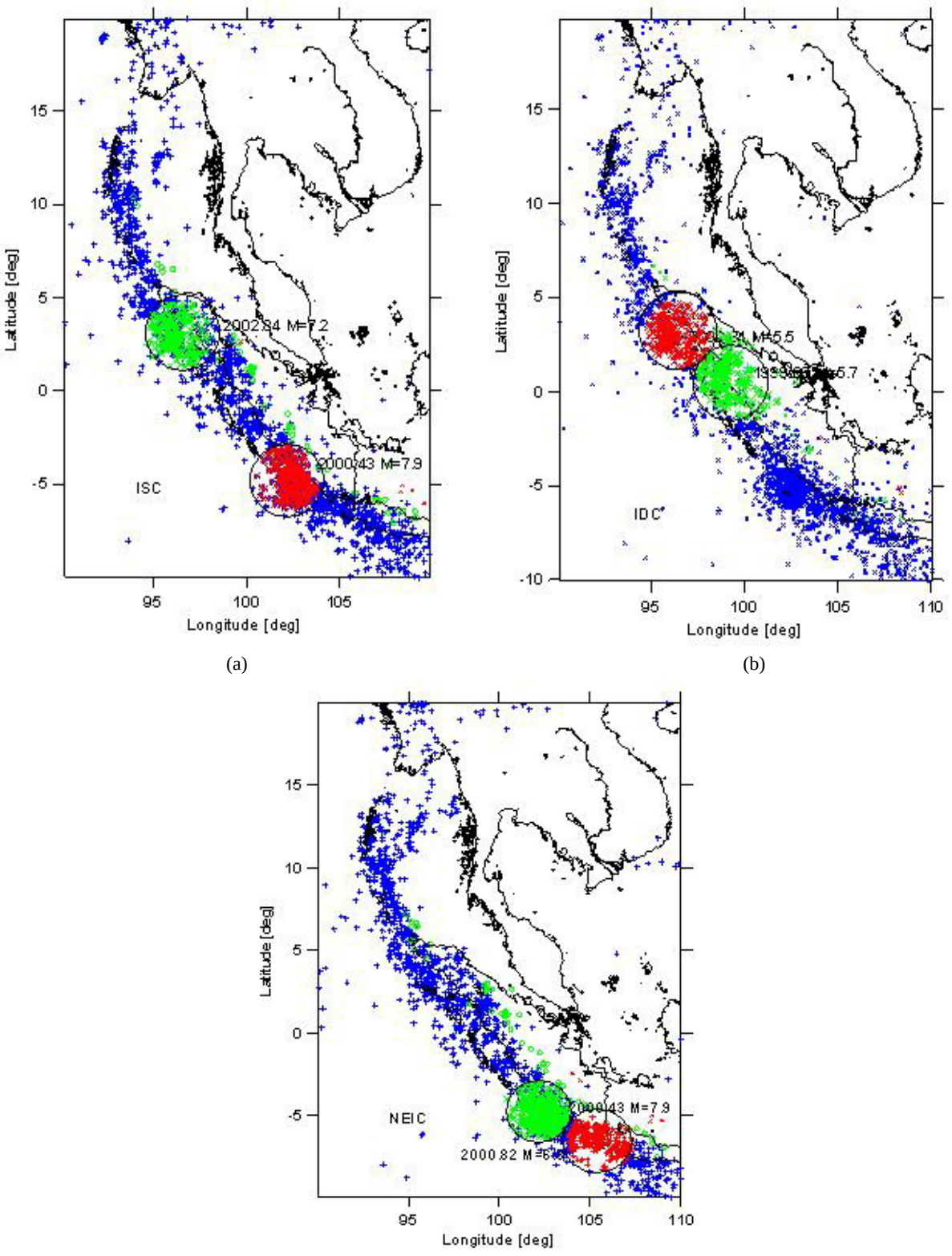

(a) (b) (c)

Fig. 9 Map of epicenters around the selected events: (a) ISC, (b) IDC and (c) NEIC catalogs. Red and green colors in black circles are epicenters within 200 km radii centered at the selected events (Table 5).

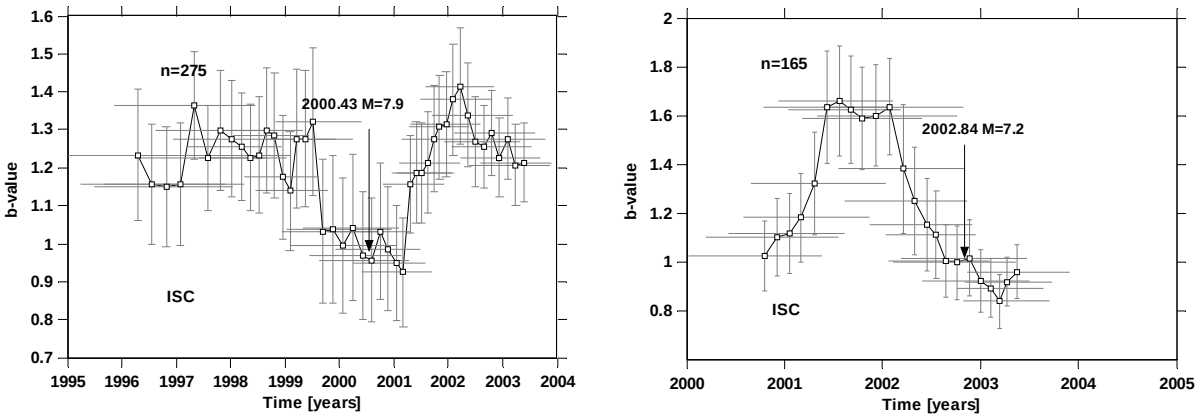

(a)

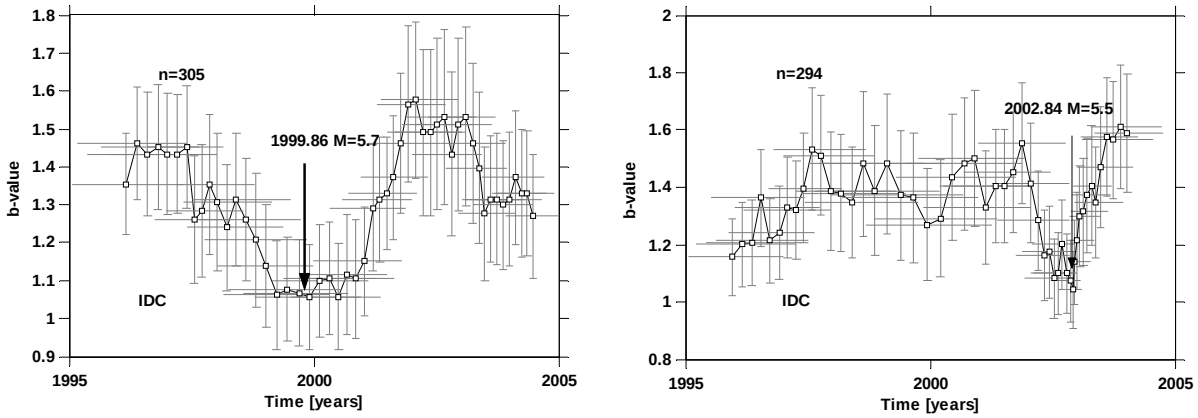

(b)

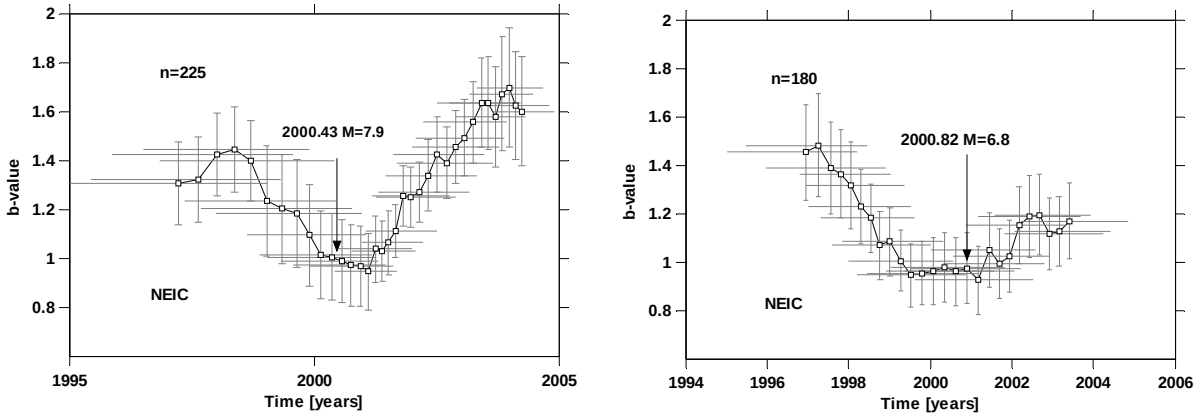

(c)

Fig. 10 Temporal variations of *b*-values for areas around the selected large events from (a) ISC, (b) IDC and (c) NEIC catalogs. Arrows indicate the time of occurrence of the events. *n* = number of events used. Vertical and horizontal bars show one standard deviation and sample period, respectively.

in the IDC catalog is higher than in the NEIC list because of the low IDC threshold magnitude. The number of events and overall *b*-value of the aftershocks from 26 December 2004 (2004.98) to the end of the reporting period of the IDC, NEIC and HRVD catalogs are 1.33, 1.31 and 1.11, respectively (Table 7). Earthquake data from the ISC is currently not available for the period after the year 2003. By comparison,

Table 6 Changes of *b* in the epicentral area, prior to the occurrence of the selected events.

Catalog	Change of *b*	
	Event 1 (Left)	Event 2 (Right)
ISC	0.4	0.6
IDC	0.4	0.4
NEIC	0.45	0.5

b-values for events preceding the 2004 shock (Table 2) are, as expected (see e.g. Ref. [48]), lower than *b*-values deduced from the aftershock series by 0.12 for IDC and NEIC and 0.14 for HRVD. The rupture of the December 26, 2004 shock propagated northward from its epicenter, from around 2°N to 15°N, i.e. from near Simeulue Island to the Andaman Islands. Nearly three months later, on March 28, 2005, a second large earthquake, M_w = 8.7, occurred about 150 km farther southeast. Aftershock series of these two events do not overlap [49], lining up in opposite directions. This behavior makes it possible to distinguish the aftershocks series of the two events and to investigate separately corresponding variations of *b* in time and space. The IDC and NEIC data are used for this investigation. Fig. 11 shows epicentral maps of the aftershocks. The red line separates the aftershocks of the December 26, 2004 and of the March 28, 2005 events. Aftershocks of the December 26 shock during the period from December 26, 2004 to March 28, 2005 are easily identified. After the occurrences of the second shock the two aftershock series mix together. In order to distinguish the two series, aftershocks that occurred after March 28, 2005 are separated into two groups by their geographical distribution and aftershocks of the December 26 shock that occurred after March 28, 2005 are combined with aftershocks from the period December 26, 2004-March 28, 2005. Fig. 12 displays epicenters of aftershocks with magnitude $M \geq M_c$ of the two events.

b-values for aftershocks of the 26 December 2004 and 28 March 2005 events are calculated for the IDC and NEIC catalogs, whereas the HRVD list is applied only for the first mainshock due to a low

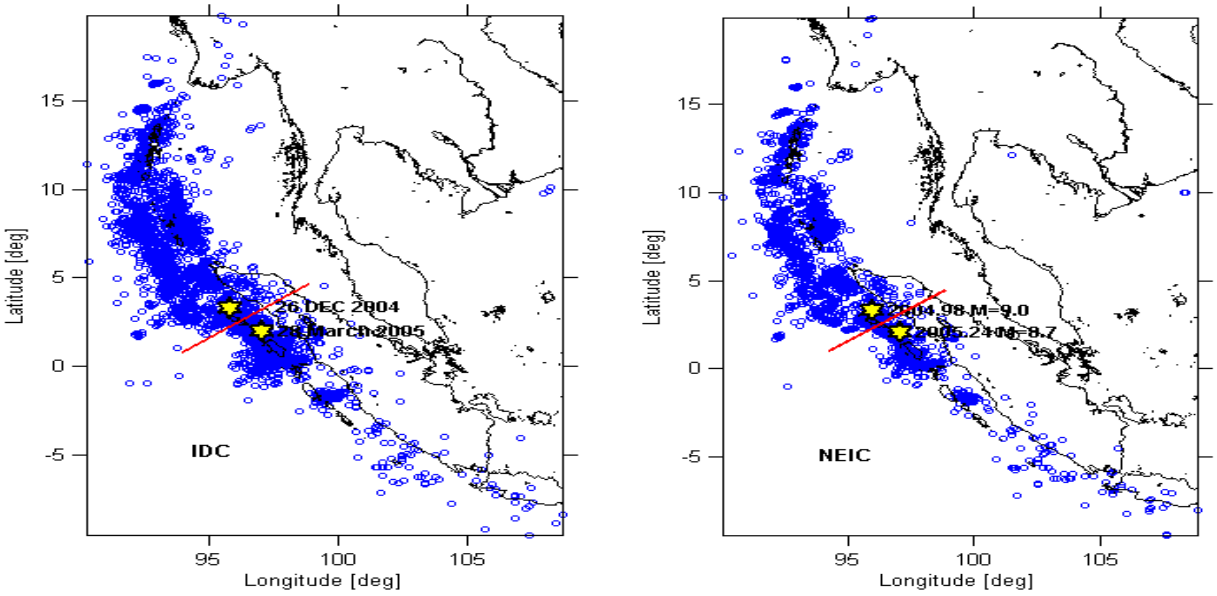

Fig. 11 Epicentral map of aftershocks reported in the IDC (left) and NEIC catalog (right). Red lines show a rough separation of two aftershocks series (for details see the text). Stars are the epicenters of the 2004 and 2005 mainshocks.

Table 7 Number of aftershocks and *b*-values for different catalogs.

Catalog	Time period	Magnitude type	Number of events	*b*-value	M_c
ISC	N/A	-	-	-	-
IDC	2004.98-2005.62	m_b	7,711	1.33 ± 0.03	3.9
NEIC	2004.98-2005.99	M_w	5,209	1.31 ± 0.02	4.6
HVRD	2004.98-2005.88	M_w	414	1.11 ± 0.01	5.2

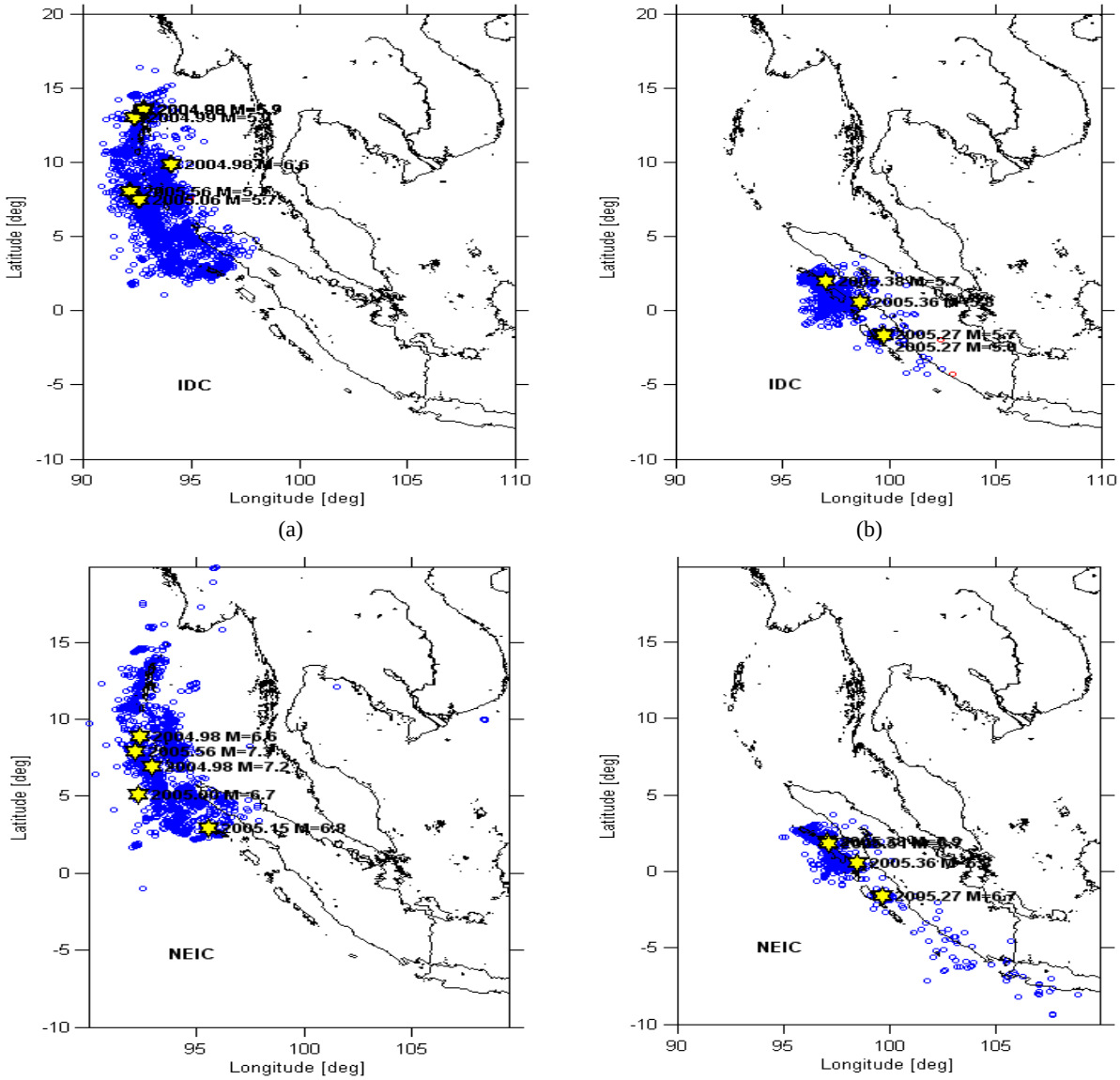

Fig. 12 Epicenter map of aftershocks ($M \geq M_c$) of the two mainshocks: (a), (c) 26 December 2004; (b), (d) 28 March 2005. Stars mark large aftershocks with magnitudes $m_b > 5.6$ and $M_w > 6.5$ in the IDC and NEIC catalogs, respectively.

number of recorded aftershocks after the second mainshock. Results are summarized in Table 8, where b_1 and b_2 are *b*-value of aftershocks for the first and the second mainshock, respectively. As follows from the table, $b_2 > b_1$. This is because the mean magnitude of aftershocks of the 28 March 2005 is lower than that of aftershocks of the 26 December 2004 (see Eq. (2)).

b-values of the two aftershock series were also investigated as functions of time and space. Changes of the *b*-value before and after the $M = 9$ giant shock in the area around the epicenter can be observed. Fig. 13 depicts *b(t)*, with arrow marks showing the position of the large aftershocks that occurred in the period between the mainshock and the end of the catalogs. Changes of *b(t)* before large events are significant, *b* changes by about 0.4-0.6, 0.4-0.8 and 0.5-1.5 for the IDC, NEIC and HRVD lists, respectively. Only two drops in the *b(t)* curve for HRVD are found due to the low number of registered events. Spatial variations of *b*-values for the IDC and NEIC catalogs are displayed in Fig. 14 and for the HRVD catalog in Fig. 15.

Table 8 ***b*-values of aftershocks of the two mainshocks: 26 December 2004 (b_1) and 28 March 2005 (b_2). n_1 and n_2 are number of events used, $M \geq Mc$.**

Catalog	n_1	b_1	n_2	b_2	M_c
IDC	2,922	1.27 ± 0.04	1,610	1.47 ± 0.03	3.9
NEIC	2,009	1.27 ± 0.03	1,114	1.34 ± 0.03	4.6
HVRD	288	1.25 ± 0.03	-	-	5.2

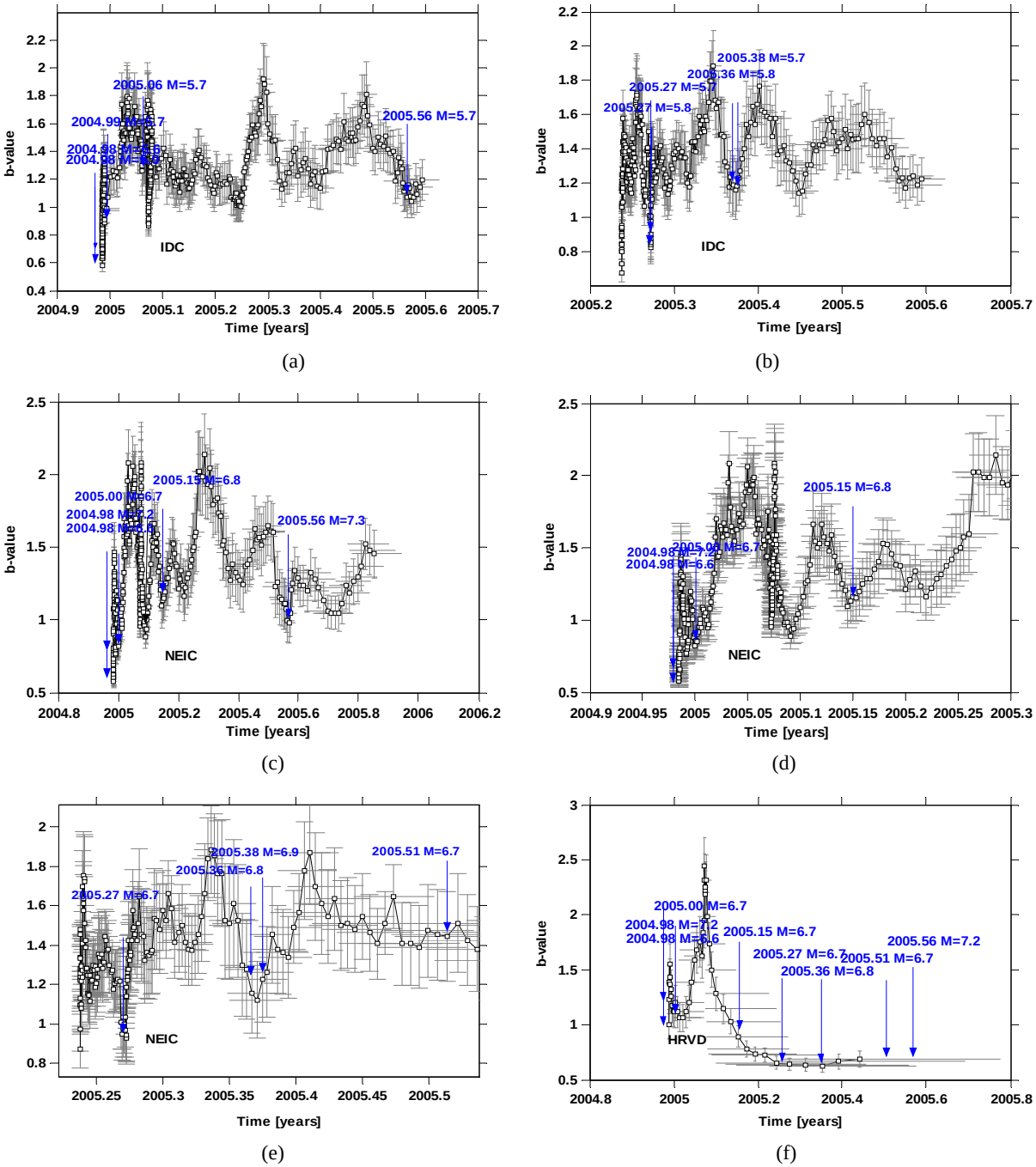

Fig. 13 ***b(t)* of the aftershocks for: the event of December 26, 2004, (a) IDC, (c) NEIC and (d) time expansion of (c); the event of March 28, 2005, (b) IDC, (e) NEIC; both mainshocks: (f) HRVD.**

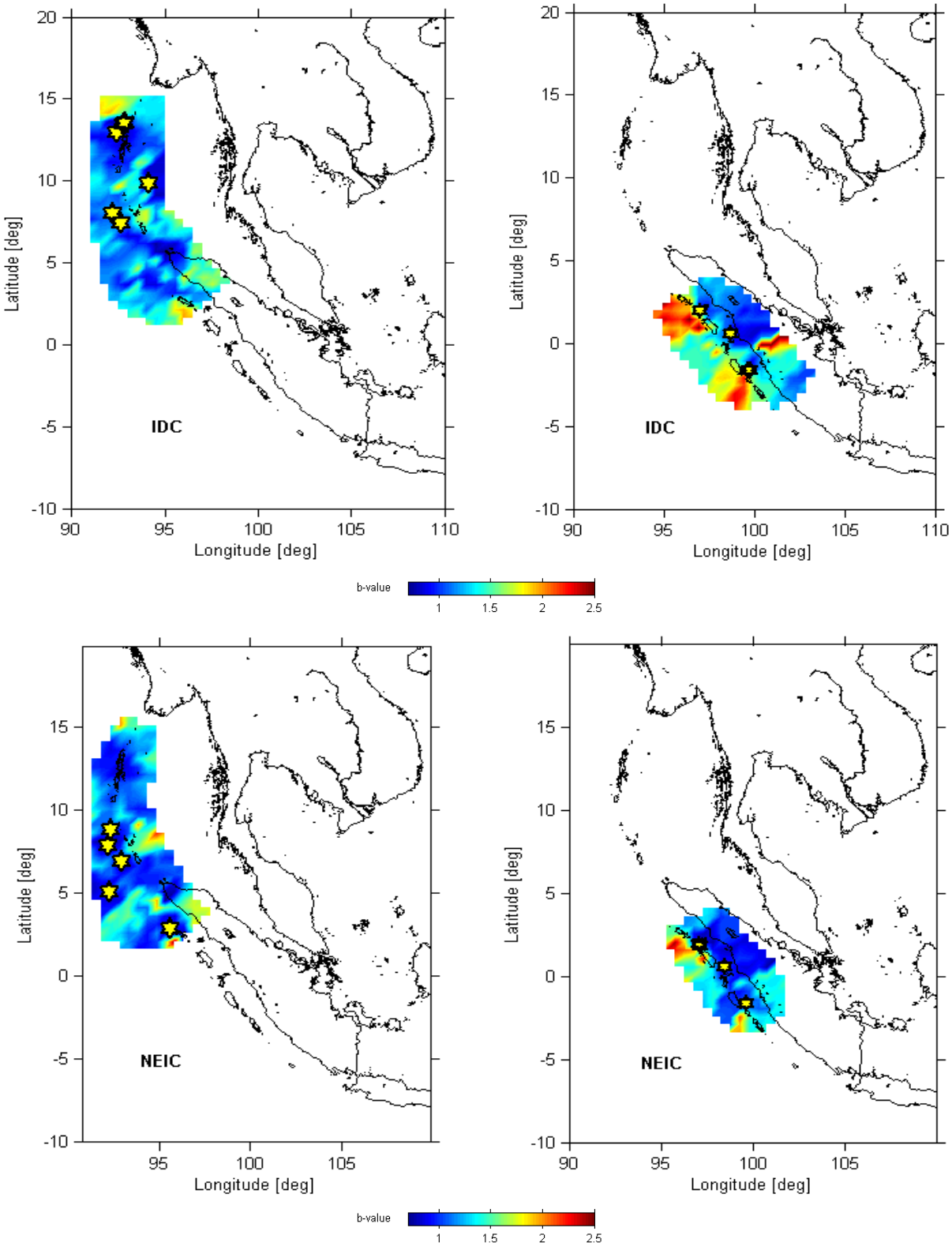

Fig. 14 ***b*-value maps of two aftershock sequences. Left: aftershocks of the December 26, 2004 event. Right: aftershocks of the March 28, 2005 event. Stars mark large aftershocks with magnitude $m_b > 5.6$ and $M_w > 6.5$, respectively for the IDC and NEIC catalogs.**

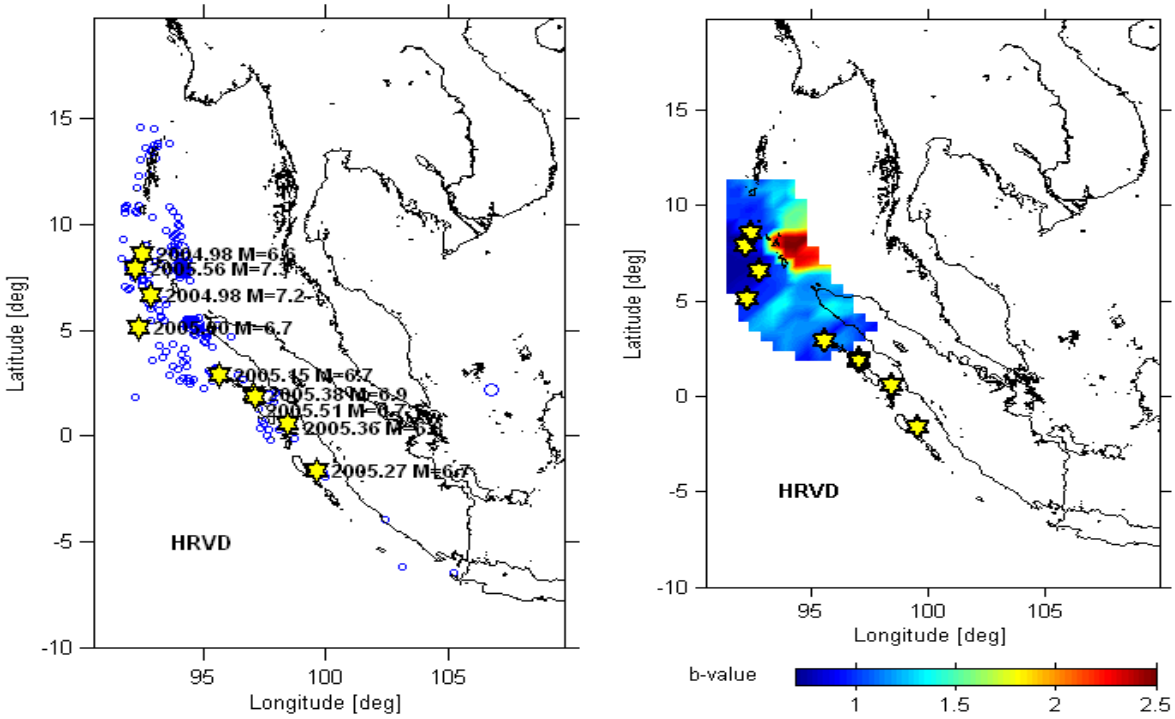

Fig. 15 Epicentral map (left) and *b*-value map (right) of aftershocks for the HRVD list. Stars mark large aftershocks, M_w > 6.5.

The mapping of *b*-values in Fig. 14 and Fig. 15 reveals a high b anomaly in the area northwest of the 26 December 2004 shock, *b*~1.2-1.5, and in the area west of the 28 March 2005 event, *b*~2-2.2. There are no large events occurring in these areas, which suggest that high stress release took place in these areas after the occurrence of the two mainshocks.

9. Conclusions

b-values characterizing the spatial and temporal variation of seismicity in the Andaman-Sumatra region during 10 years before the giant shocks of December 26, 2004 and March 28, 2005 were calculated using earthquake data from four (ISC, IDC, NEIC and HVRD) different earthquake catalogs. Data from each catalog have been carefully selected and analyzed. Completeness of the catalogs is an important parameter that has to be taken into consideration in the determination of *b*. Analysis using longer time periods is not suitable because the threshold magnitude, M_c, of most networks changes with time, due to network upgrading and improvement of analysis methods. During the earlier period M_c is high, therefore by using a longer time period the average high M_c will cause loss of a number of earthquakes. Different magnitude scales can be used in the estimation of *b*-value and results are comparable.

A five-year period of earthquake data is suitable to study changes of *b*-value both temporally and spatially, provided there are adequate earthquake data in the catalogs. Results from two consecutive five-year periods reveal that low *b*-value anomalies appear in areas of large future earthquakes. Three major changes of *b* were found at latitudes 0°-15°N, i.e. north of the 2004 giant shocks, at 4°S-2°N i.e. around the epicenter of the M = 8.7 event and at 5°S-7°S. *b*-value mapping reveals information about the condition of the crust in the subduction zone and active faults. The resolution of spatial mapping depends on earthquake density in the area. The available data generally provides a resolution of between 50 and 200 km.

Variation in *b(t)* shows that the large events occurred in intervals of low *b*-value i.e. about 0.3-1. A rapid increase of *b(t)* is observed after the occurrence of large

earthquakes. This analysis suggests that changes of *b*-value can be used as earthquake medium-term (months-years) precursor. Precursory time prior to a large event depends on the resolution of *b(t)* which in turn depends on M_c or the detection ability of the network.

Results from aftershocks series analysis in both time and space are also convincing as for the mainshocks. After the occurrence of the two giant $M_w = 9$ and $M_w = 8.7$ earthquakes, stress changes from high to low (*b* changes from low to high) in the epicentral areas and their surroundings. *b*-value of aftershocks increases by about 0.12 for IDC and NEIC and by 0.14 for HRVD data.

Acknowledgments

This work has been conducted at the Department of Earth Sciences, Seismology, Uppsala University, Persson for guidance and valuable suggestions. Thanks to Prof. R. Roberts and Prof. Allen J. Anderson for careful reading and thoughtful comments that improved the manuscript. The work was supported by the ISP (International Science Program) Uppsala University. Sincere thanks go to Dr. S. Weimer, EHT, Zurich, Switzerland for providing the ZMAP software and for training. Earthquake data used in this study were compiled from the International Seismological Centre (ISC), the International Data Centre (IDC), the National Earthquake Information Center (NEIC) and the Harvard Seismology Group (HRVD).

References

[1] Y. Ogata., M. Imoto, K. Katsura, 3-D spatial variation of *b*-values of magnitude-frequency distribution beneath the the Kanto district, Japan, Geophys. J. Int. 143 (1991) 135-146.

[2] K. Mogi, Seismicity before and after large shallow earthquakes around the Japanese islands, Tectonophysics 175 (1990) 1-33.

[3] R. Jain, B.K. Rastogi, C.S.P. Sarma, Precursory changes in source parameters for the Koyna-Warna (India) earthquakes, Geophys. J. Int. 158 (2004) 915-921.

[4] T.I. Urbancic, R.P. Young, Space-time variations in source parameters of mining-induced seismic events with $M < 0$, Bull. Seis. Soc. Am. 83 (1993) 378-397.

[5] F.F. Evison, D.A. Rhoades, The precursory earthquake swarm in New Zealand: hypothesis tests, New Zealand J. Geol. and Geophys. 36 (1993) 51-60.

[6] F.F. Evison, D.A. Rhoades, The precursory earthquake swarm in New Zealand: Hypothesis tests II, New Zealand J. Geol. and Geophys. 40 (1997) 537-547.

[7] F.F. Evison, D.A. Rhoades, The precursory earthquake swarm and the inferred precursory quarm, New Zealand J. Geol. and Geophys. 42 (1999) 229-236.

[8] G. Molchan, O. Dmitrieva, Dynamic for the magnitude-frequency relation for foreshocks, Phys. Earth Planet. Inter. 61 (1990) 99-112.

[9] B. Gutenberg, C.F. Richter, Frequency of earthquakes in California, Bull. Seismol. Soc. Am. 34 (1944) 185-188.

[10] P.M. Hatzidimitriou, E.E. Papadimitriou, D.M. Mountrakis, B.C. Papazachos, The seismic parameter *b* of the frequency-magnitude relation and its association with the geological zones in the area of Greece, Tectonophysics 120 (1985) 141-151.

[11] T. Tsapanos, *b*-values of two tectonic parts in the circum-Pacific belt, Pageoph. 134 (1990) 229-242.

[12] A.M.S. Al-Amri, B.T. Punsalan, E.A. Uy, Spatial distribution of the seismicity parameters in the Red Sea regions, J. Asian Earth Sci. 6 (1998) 557-563.

[13] D. Schorlemmer, S. Wiemer, M. Wyss, Variation in earthquake-size distribution across different stress regimes, Nature 437 (22) (2005) 539-542.

[14] K. Aki, Maximum likelihood estimate of *b* in the formula $\log N = a - bM$ and its confidence limits, Bull. Earthquake Res. Inst., Tokyo Univ. 43 (1965) 237-239.

[15] A. Yilmaztürk, P.W. Burton, An evaluation of seismic hazard parameters in southern Turkey, J. Seismology 3 (1999) 61-81.

[16] C. Frohlich, S. Davis, Teleseismic *b*-values: Or, much ado about 1.0, J. Geophys. Res. 98 (1993) 631-644.

[17] M. Westerhaus, M. Wyss, R. Yilmaz, J. Zschau, Correlating variations of *b*-values and crustal deformations during the 1990s may have pinpointed the rupture initiation of the $Mw = 7.4$ Izmit earthquake of 1999 August 17, Geophys. J. Int. 148 (2002) 139-152.

[18] S. Wiemer, M. Wyss, Mapping the frequency-magnitude distribution with depth in two volcanic areas: Mount St. Helens, Washington, and Mount Spurr, Alaska, Geophy. Res. Lett. 24 (1997) 189-192.

[19] C.H. Scholz, The frequency-magnitude relation of microfracturing in the rock and its relation to earthquake, Bull. Seismol. Soc. Am. 58 (1968) 399-415.

[20] M. Imoto, Changes in the magnitude-frequency *b*-value prior to large ($M \geq 6$) earthquakes in Japan, Tectonophysics 193 (1991) 311-325.

[21] O.P. Sahu, M.M. Saikia, The *b*-value before the 6th

August, 1988 India-Myanmar border region earthquake-A case study, Tectonophysics 234 (1994) 349-354.

[22] Y. Shi, B.A. Bolt, The standard error of the magnitude-frequency *b*-value, Bull. Seismol. Soc. Am. 72 (1982) 1677-1687.

[23] T. Eguchi, S. Uyeda, T. Maki, Seismotectonics and tectonic history of the Andaman Sea, Tectonophysics 57 (1979) 35-51.

[24] M.R. Kumar, N. Purnachandra Rao, S.V. Chalam, A seismotectonic study of the Burma and Andaman arc regions using centroid moment tensor data, Tectonophysics 253 (1996) 155-165.

[25] S. Dasgupta, M. Mukhopadhyay, Seismicity and plate deformation below the Andaman arc, northeastern Indian Ocean, Tectonophysics 225 (1993) 529-542.

[26] P. Nuannin, O. Kulhánek, L. Persson, Spatial and temporal *b*-value anomalies preceding the devastating off coast of NW Sumatra earthquake of December 26, 2004, Geophys. Res. Lett. 32 (2005) 4.

[27] K.A. Raju Kamesh, T. Ramprasad, P.S. Rao, B. Ramalingeswara Rao, J. Varghese, New insights into the tectonic evolution of the Andaman basin, northeast Indian Ocean, Earth Plan. Sci. Lett. 221 (2004) 145-162.

[28] C.R. Scotese, L.M. Gahagan, D.R.L. Larson, Plate tectonic reconstruction of the Creataceous and Cenozoic ocean basins, Tectonophysics 155 (1988) 27-48

[29] S. Dasgupta, Seismotectonics and stress distribution in the Andaman Plate, Mem. Geol. Soc. India 23 (1992) 319-334.

[30] M. Pubellier, C. Monnier, R. Maury, D.R. Tamayo, Plate kinematics, origin and tectonic emplacement of supra-subduction ophiolites in SE Asia, Tectonophysics 392 (2004) 9-36.

[31] D.E. Karig, S. Suparka, G.F. Moore, P.E. Hehanusa, Structure and Cenozoic evolution of the Sunda arc in the central Sumatra region, in: J. Watkin, L. Montadert, P.W. Dickenson (Eds.), Geological and Geophysical Investigations of Continental Margins, 1979, pp. 223-237.

[32] T.J. Fitch, Plate convergence, transcurrent faults and internal deformation adjacent to SE Asia and Western Pacific, J. Geophys. Res. 77 (1972) 4432-4460.

[33] J.R. Curray, The Sunda arc: A model for oblique convergence, Netherlands J. Sea Res. 24 (2/3) (1989) 131-140.

[34] J.R. Curray, Tectonics and history of the Andaman Sea region, J. Asian Earth Sci. 25 (2005) 187-232.

[35] A. Udías, Principle of Seismology, Cambridge University Press, 1999, p. 475.

[36] P.A. Reasenberg, Second-order moment of central California seismicity, J. Geophys. Res. 90 (1985) 5479-5495.

[37] S. Wiemer, R.F. Zuniga, , ZMAP-A software package to analyze seismicity, EOS, Trans. Fall Meeting, AGU 75 (1994) 456.

[38] S. Wiemer, M. Wyss, Minimum magnitude of completeness in earthquake catalogs: Eaxamples from Alaska, the weatern US and Japan, Bull. Seismol. Soc. Am. 90 (2000) 859-869.

[39] D. Schorlemmer, G. Nari, S. Weimer, A. Mostaccio, Stability and singnificant tests for *b*-value anomalies: Example from the Tyrrhenian Sea, Geophys. Res. Lett. 30 (16) (2003) 4.

[40] S.J. Gibowicz, S. Lasocki, Seismicity induced by mining: Ten years later, Adv. Geophys. 44 (2001) 39-181.

[41] P. Nuannin, O. Kulhánek, L. Persson, K. Tillman, Forecasting of increased induced seismicity in the Zinkgruvan Mine, Sweden, by using temporal variations of *b*-values, Acta Montana Journal, Ser. A 21 (125) (2002) 13-25.

[42] P. Nuannin, O. Kulhánek, L. Persson, T. Askemur, Inverse correlation between induced seismicity and *b*-value, observed in the Zinkguvan mine, Sweden, Acta Geodyn. Geomater. 2 (140) (2005) 5-13.

[43] S. Wiemer, M. Wyss, Mapping spatial variability of the frequency-magnitude distribution of earthquakes, Adv. Geophys. 45 (2002) 259-302.

[44] L.M. Jones, E. Hauksson, The seismic cycle in southern California: Precusor or response?, Geoph. Res. Lett. 24 (1997) 469-472.

[45] D.J. Varnes, Predicting earthquakes by analyzing accelerating precursory seismic activity, Pure Appl. Geophys. 130 (1989) 661-686.

[46] D.A. Monterroso, O. Kulhánek, Spatial variations of b-values in the subduction zone of Central America, Geofisica Int. 42 (4) (2003) 1-13.

[47] S. Wiemer, A software package to analyze seismicity: ZMAP, Seism. Res. Lett. 72 (2001) 373-382.

[48] F. Koyama, The Complex Faulting Process of Earthquakes, Kluwer Academic Publishers, 1997, p. 194.

[49] S.C. Singh, Sumatra earthquake research indicates why rupture propagated northward, EOS Trans. Am. 86 (48) (2005) 497-502.